*COLLOID JOURNAL, 2025, Vol. 87, No. 1, pp. 3–14*

# EFFECT OF CONDITIONS FOR OBTAINING DETONATION NANODIAMOND ON SURFACE COMPOSITION AND STABILITY OF ITS AQUEOUS SOLS[1]

**© 2025 A. V. Volkova*, D. A. Savelev, N. S. Chuikov, V. A. Vodolazhskii, and L. E. Ermakova**

*Saint Petersburg State University, Saint Petersburg, Russia*

**e-mail: anna.volkova@spbu.ru*

Received November 15, 2024
Revised December 08, 2024
Accepted December 19, 2024

**Abstract.** In present work, the effect of additional treatment of detonation nanodiamond (DND) powder of basic purification on the surface composition of DND particles, their electrokinetic properties, as well as aggregate stability in solutions of indifferent electrolyte (NaCl) in a wide pH range was studied. It has been found that a higher degree of purification of the samples and an increase in the number of protonated carboxyl groups on the surface of the DND particles due to additional acid and thermoammonia treatment leads to a shift in the position of the isoelectric point (IEP) from pH 7.0 for the initial sample to pH 6.3 and pH 6.0, respectively. It is shown that the coagulation thresholds of hydrosols at natural pH and the position of stability zones in $10^{-3}$ M sodium chloride solution are in full compliance with the IEP values. The highest thresholds are observed at pH 5.8 for the initial DND, while for the dispersion of DND particles after thermoammonia treatment, fast coagulation occurs already at a concentration of $10^{-4}$ M. It is also shown that the aggregate stability zones for additionally treated DND samples almost coincide. In the case of DND of basic purification, the stability zone expands in the area of positive zeta-potential, and in the area of negative values stability is not observed, probably due to the partial dissolution of surface impurities at high pH and their transition in ionic form to the solution, which causes coagulation of DND particles.

**Keywords:** *detonation nanodiamond, surface modification, surface functional groups, aggregate stability, coagulation threshold, zeta-potential, isoelectric point*

**DOI:** 10.31857/S002329122501016e6

## INTRODUCTION

Detonation nanodiamonds, due to such classical properties of diamond as hardness and chemical inertness, are widely used as materials for finishing polishing, in electroplating, and in oil compositions [1, 2]. It is possible to use DND as sorbents with ion exchange properties [3–5]. In recent years, DND nanoparticles have attracted increasing interest due to the prospect of their use in biomedical applications [6–9]. The possibility of effective practical application of both dilute and concentrated dispersions of DND is largely determined by their electrosurface properties, as well as sedimentation and aggregation stability, which depend on the surface composition and, consequently, on the conditions of detonation nanodiamond production. In this case, sedimentation stability in concentrated dispersions (for example, when obtaining polishing compositions) can be achieved due to the formation of periodic colloidal structures, i.e., due to the loss of aggregative stability by the system [10]. The position of the zero charge point and isoelectric point, and, consequently, the sorption properties and values of the electrokinetic potential of DND particles, other things being equal, can be influenced by refining DND base powders from both surface impurities, including water-soluble metal-containing impurities [11, 12], and non-diamond forms of carbon. Unification of the detonation nanodiamond surface, often leading to disaggregation of powders due to the removal of at least most of the $sp^2$-carbon, is performed by chemical and/or thermal treatment of DND both basic and deep purification: most often by

[1] Supplementary materials can be found at the DOI page of the article: https://doi.org/10.31857/S002329122501016e6

oxidation or reduction in the liquid or gas phase (air, ozone, argon, hydrogen) [13–20]

In addition, aqueous DND sols can serve as a model system for studying the electrokinetic characteristics and the structure of the boundary layer depending on the functional composition of the surface in contact with the electrolyte solution, as well as the regularities of aggregation in nanodisperse systems [21] containing both nanoparticles and primary aggregates. Such fundamental studies are important both for the improvement of theoretical ideas about the structure of the electrical double layer at the solid-solution interface and for the development of existing theories of the stability of real dispersions. It should be noted that most of the works devoted to the study of electrokinetic properties and stability of DND sols consider systems in which the sign of the surface charge of DND particles does not change practically in the whole pH region [22–28]. In turn, the IEP position in the neutral pH region (as in the case of DND powders studied in the present work) makes it possible to study the coagulation behavior of sols depending on their colloidal-chemical properties, both in the positive and negative surface charge region. From the point of view of applied problems such DND powders depending on pH can be used, for example, as sorbents for the extraction of both cationic and anionic impurities from the liquid phase, to form various kinds of coagulation structures in concentrated dispersions.

In connection with the above, the aim of the present work was to investigate the aggregative stability of aqueous sols of industrial DND powders (basic and additional acid and thermoammonia purification) in a wide range of concentrations and pH of sodium chloride solutions, as well as to establish the relationship between the conditions of their production, composition of the surface, electrokinetic properties and the position of stability and coagulation zones of detonation nanodiamond hydrosols.

## EXPERIMENTAL PART

As an object of study we used industrial detonation nanodiamond powder produced by FSUE SCTB "Technolog" (St. Petersburg, Russia), obtained by detonation of TNT–hexogen mixture in the ratio 60/40 and separated from the diamond-containing charge by thermoxidation with aqueous ammonium nitrate solution with nitric acid additives according to the method presented in the patent RU2599665C2. The sample is labeled in the article as DND. To establish the relationship between the conditions of purification and unification of the surface of DND powders and the aggregative stability of dispersions obtained from them, SCTB "Technolog" also provided samples of detonation diamond obtained from the initial DND of basic purification ("raw material") by additional thermoammonia treatment (DND-TA) and treatment with a mixture of nitric (56%) and hydrofluoric (40%) acids (DND-A) at room temperature.

To remove possible ionic impurities remaining after chemical treatment of DND powders, all provided samples were purified three times by electrodialysis. The purification cycle is described in detail in [29].

The specific surface area values $S_{sp}$ of the powders were determined by BET method by thermal desorption of nitrogen with chromatographic registration. The average size of primary nanoparticles $d_o$ was calculated by the formula:

$$d_o = 6/\rho S_{sp}, \quad (1)$$

where $\rho = 3.52$ g/cm$^3$ is the density of DND.

The phase composition of the powders was determined at the Resource Center (RC) for X-ray Diffraction Studies using a Bruker "D2 Phaser" desktop automatic powder diffractometer (Bruker AXS, Germany). Phase identification was carried out with the help of the PDXL 2.0 software package using the Powder Diffraction File database (PDF-2 Release 2020 RDB, PDF-2/Release 2011 RDB).

Elemental analysis of DND powders was performed by X-ray photoelectron spectroscopy (XPS) using a Thermo Fisher Scientific Escalab 250Xi integrated photoelectron and scanning Auger-electron spectrometer (Thermo Fisher Scientific, UK) in the Resource Center for Physical Methods of Surface Investigation of the SPSU Science Park and energy dispersive X-ray fluorescence spectroscopy on a Shimadzu EDX-800P spectrometer (Shimadzu, Japan) in the RC for Innovative Technologies of Composite Materials of the SPSU Science Park.

The surface composition of DND particles was also studied by Raman methods on a Senterra instrument (Bruker, Germany) in backscattering geometry and disturbed total internal reflection (DTIR) on a Nicolet 8700 FT-IR spectrometer (Thermo Scientific, USA) with a DTIR attachment (Smart iTR) with a diamond crystal at the Resource Center for Optical and Laser Materials Research of the SPSU Science Park. Raman excitation was performed using an external solid-state laser with a wavelength of 532 nm. Spectra were recorded in the range of 100–2,200 cm$^{-1}$. The IR absorption spectra after subtraction of the base line caused by scattering were given by the maximum value in the region of valence vibrations of OH-groups.

To study the electrokinetic properties and aggregative stability of aqueous dispersions of detonation nanodiamond as a function of the concentration of sodium chloride solutions ($10^{-4}$–$10^{-1}$ M) at natural pH (5.8–6.0) and pH (4–11.5) in $10^{-3}$ M NaCl solution, dilute hydrosols of DND were prepared according to the method [29], which retained their dispersibility throughout the experiment. The particle sizes of the initial aqueous DND hydrosols are given in Table 1.

It should be noted that the obtained initial sols diluted twice with deionized water had similar values of optical density (0.19 ± 0.01 at a light wavelength of 380 nm) and partial concentration $(2–4)\times10^{10}$ particles/cm$^3$, determined by particle trajectory analysis on a NanoSight NS300 device (Malvern, UK).

Particle sizes of DND hydrosols were determined by scanning electron microscopy (SEM) using a Carl Zeiss Merlin scanning electron microscope (Carl Zeiss Merlin, Germany) in the Interdisciplinary Resource Center for Nanotechnology at the SPSU Science Park and by dynamic light scattering (DLS) on a Zetasizer Nano ZS analyzer (Malvern Instruments, UK) in a universal capillary U-shaped cuvette (DTS1070) with integrated gold-plated electrodes with pre-tempering for 2 min at 20°C.

To study the coagulation process of DND sols, turbidimetry methods were used (the detailed experimental procedure is described in [29]) using a photoelectrocalorimeter KFK-3-01 (optical path 50 mm, light wavelength 380 nm) and dynamic light scattering. Measurements of optical density were carried out within 15 minutes from the moment of electrolyte addition to the ash, particle size after 20 minutes after system creation.

The electrophoretic mobility ($U_e$) of DND particles was determined by laser Doppler electrophoresis on a Zetasizer Nano ZS analyzer (Malvern Instruments, UK) in parallel with the measurement of particle size distributions under similar conditions. The values of electrokinetic potential ($\zeta^S$) in the first approximation were calculated by the Smoluchowski equation:

$$\zeta^S = \frac{\eta}{\varepsilon\varepsilon_0}U_e \,. \qquad (2)$$

Deionized water with specific conductivity not exceeding $1.5\times10^{-6}$ Ohm$^{-1}$cm$^{-1}$ (Aqualab AL Plus water purification system) was used to prepare solutions and dispersions. The required pH values were set using $3\times10^{-2}$ M and $10^{-1}$ M solutions of hydrochloric acid and sodium hydroxide. pH of the medium was measured using a SevenMulti pH meter (Mettler Toledo).

## RESULTS AND DISCUSSION

### *Phase composition and surface composition of DND particles.*

Fig. 1 shows the results of X-ray phase analysis (XRD) of the investigated DND powders. It can be seen that in addition to the main phase of diamond on the XRD there are also weak peaks of impurity phases, which most likely belong to the phases of zinc sulfide and titanium dioxide in the modification of rutile. It can also be seen that according to the intensity of these peaks, the content of impurity phases is maximum in the initial sample of DND, while phase ZnS and phase $TiO_2$ are practically undetectable in the DND-TA sample and in the powder DND-A, respectively. In this connection, it should be noted that each method of additional processing is somewhat selective with respect to surface impurities.

The results of energy-dispersive X-ray fluorescence analysis showed (Fig. 2) that additional treatment of the initial powder of detonation nanodiamond leads to an increase in the relative content of such elements as iron (especially in the case of DND-TA) and titanium due to the partial removal from the surface of DND particles, apparently, more acid- and alkali-soluble components: calcium, silicon, aluminum, etc. The higher total content of iron and titanium elements in the DND-TA sample compared to DND-A may indicate a more effective purification in the general case of thermoammonia treatment. At the same time, the observed lowest content of zinc and sulfur for the DND-TA sample is in good agreement with the XRD results.

Fig. 3 shows the FT-IR spectra of the investigated DND powders. It can be seen that for all three samples at 1,325 cm$^{-1}$ nanodiamond peak corresponding to the valence vibration of the C–C bond in the DND crystal lattice is observed [30, 31]. It can also be seen that the main differences in the spectra of the samples are observed in the range 1,330–1,800 см$^{-1}$. Thus, the noticeable absorption at 1,350 cm$^{-1}$ for the original sample, which is most likely due to symmetric vibrations of the deprotonated carboxyl group ($COO^-$) [17], is much less pronounced for DND-TA and is practically absent in the spectrum of the DND-A sample. The change in the ratio of intensities of the peak at 1,735 cm$^{-1}$, which characterizes the valence vibrations of the carbonyl group C=O as part of the protonated carboxyl group, and the peak at 1,555 cm$^{-1}$, which can be attributed to asymmetric valence C=O vibrations as part of the deprotonated $COO^-$ group, attracts attention.

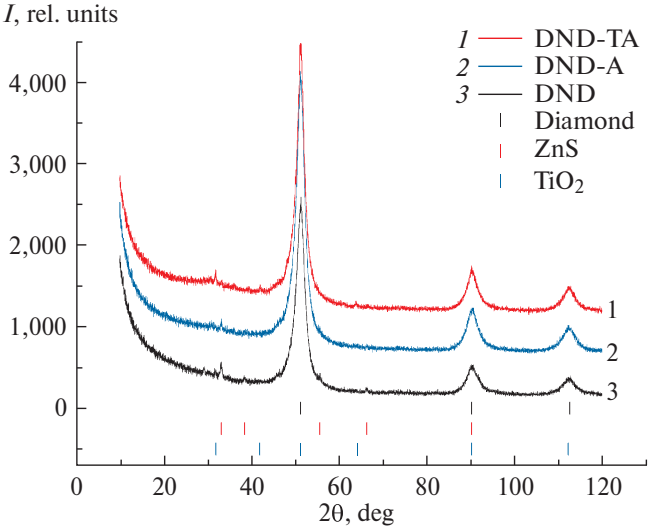


**Fig. 1.** X-ray radiographs of detonation nanodiamond powders.

**Table 1.** Structural characteristics of initial diluted aqueous DND sols.

| Sample | DND | DND-A | DND-TA |
|---|---|---|---|
| SEM images | 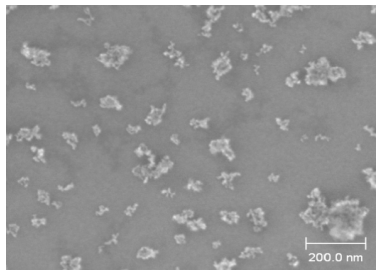  | 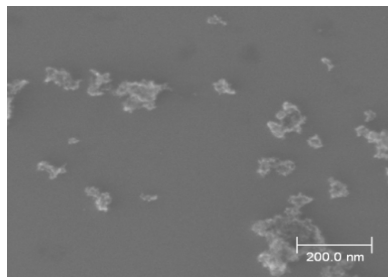  | 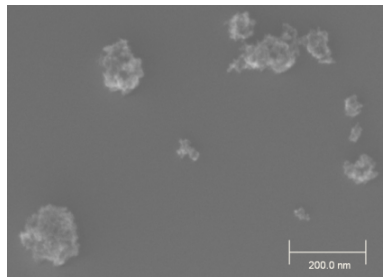  |
| Specific surface area $S_{sp}$, $m^2/g$ | 305 | 295 | 290 |
| Average size of primary nanoparticle $d_o$, nm (equation 1) | 5.6 | 5.8 | 5.9 |
| Average size (range of particle sizes) determined by DLS method $d_I$/ $d_V$ / $d_N$[1], nm | 135 (45–400)/ 85 (40–340)/ 65 (40–190) | 140 (45–340)/ 110 (40–400)/ 70 (40–255) | 180 (80–400)/ 135 (70–400)/ 110 (70–300) |

1 $d_I$ is the average particle size (diameter) from the size distribution of scattered light intensity
$d_V$ and $d_N$ are the average particle size (diameter) from the volume and particle number size distributions, respectively.

Probably due to the binding of some of the carboxyl groups to impurities, the number of deprotonated carboxyl groups on the surface of the base purification DND particles is greater than the protonated ones. Additional chemical treatment leading to the removal of part of these impurities from the surface leads to an increase in the number of protonated and a decrease in the number of deprotonated carboxylic groups, with the maximum $COOH/COO^-$ ratio observed for the DND-TA sample.

Another possible reason for the increase in the number of COOH groups for additionally treated samples is probably a decrease in the amount of $sp^2$-carbon on the surface of DND particles due to the oxidation of C=C bonds. Thus the absorption band 1,555 $cm^{-1}$ may also correspond to a possible, but less intense than C=O valence vibrations in C=C bonds, the presence of which is also confirmed by the Raman spectroscopy results.

As can be seen from Fig. 4, in addition to the nanodiamond peak at 1,328 $cm^{-1}$ [32] in the Raman spectra, there is a broad asymmetric peak with a maximum at 1,620 $cm^{-1}$, corresponding to carbon in $sp^2$-hybridization. Upon decomposition of this peak (on the example of DND-A, Fig. P1 of the Appendix), D- and G-lines of graphite are observed for all samples. It should be noted that the appearance of the graphite D-line in the Raman spectrum of DHA is associated in the literature with the formation of onion-like carbon shells around the diamond nucleus, on which the inclusions of graphite-like phase are located [33, 34]. The greater intensity of the graphite D-line in the spectrum of DND-TA compared to the original DND and DND-A (Fig. 4), apparently, characterizes the lower ordering and greater defectivity of the graphite-like phase in DND-TA. This probably indicates a more efficient removal of impurities contained in this phase from the surface of DND-TA particles, which confirms the results described above. It should also be noted that in the Raman spectra of all DND powders a peak at 1,735 $cm^{-1}$ characterizing vibrations in the C=O bond is observed.

The X-ray photoelectron spectra of the C1s of DND powders are shown in Fig. 5. It can be seen that the C1s spectrum for the basic-cleaned DND powder is shifted to the region of higher binding energies compared to the additionally treated samples. The results of deconvolution of C1s peaks for DND and DND-A powders (similarly for DND-TA) (Fig. 6) showed that all samples are characterized by the presence of a peak with energy 287.7 ± 0.1 eV, corresponding to the C=O bond in the carbonyl [35, 36] or carboxyl group [14], and a peak 286.7 ± 0.1 eV corresponding to the C–O bond in hydroxyl and ether groups [14, 35–37] and probably to the C–N and C=N bonds according to [32, 38] and N1s spectra data (peak 399.3 eV, Fig. P2 of the Appendix). The peak at a binding energy of 403.1 eV probably characterizes the bonding of a nitrogen atom with three neighboring carbon atoms [32]. The least intense peak at a binding energy of 288.8 eV, appearing only in the spectrum of the initial DND (Fig. 6a), is often attributed to the carbon-oxygen bond in the COOH-group [39]. It can also be seen that, while the peak at 286.7 eV is the most intense for the original sample, for the DND-TA and DND-A samples (Fig. 6b) the main peak corresponds to a binding energy of 285.5 eV, corresponding to $sp^3$-hybridized carbon in the diamond crystal lattice, which is absent in the spectrum of the original sample. The observed changes in the C1s spectrum of the original sample after additional acid or thermoammonia treatment indicate a deeper purification of the samples from the non-diamond phase and, first of all, summarizing

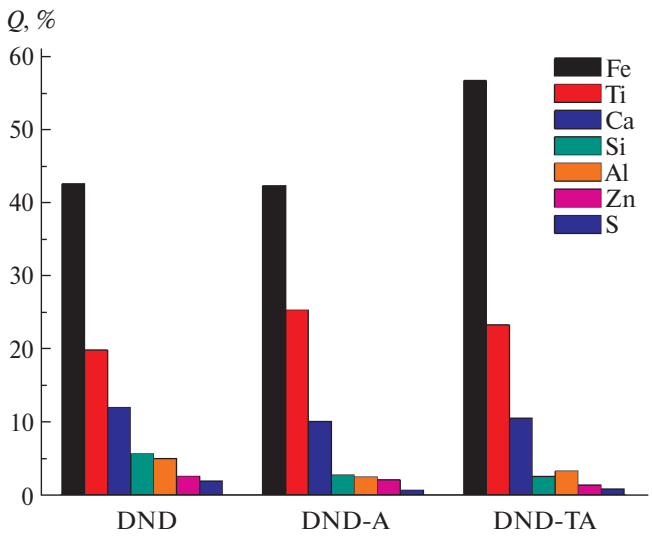


**Fig. 2.** Relative content of some elements on the surface of DND particles.

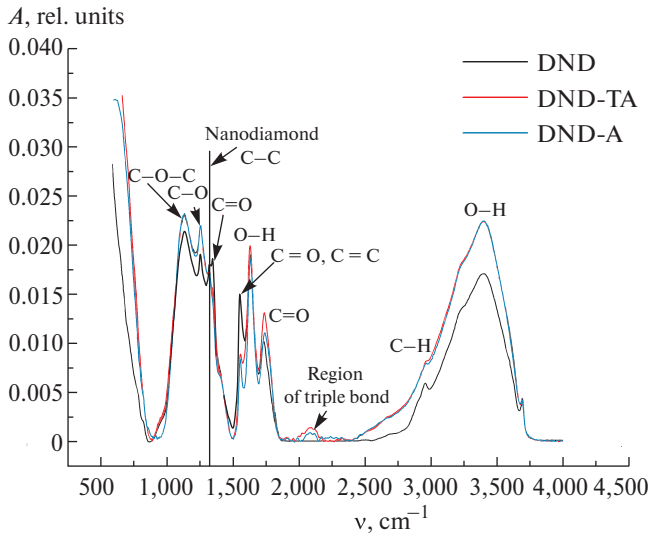


**Fig. 3.** Infrared absorption spectrum of DND powders with base line subtraction and fitting to the maximum in the valence vibration region of OH-groups.

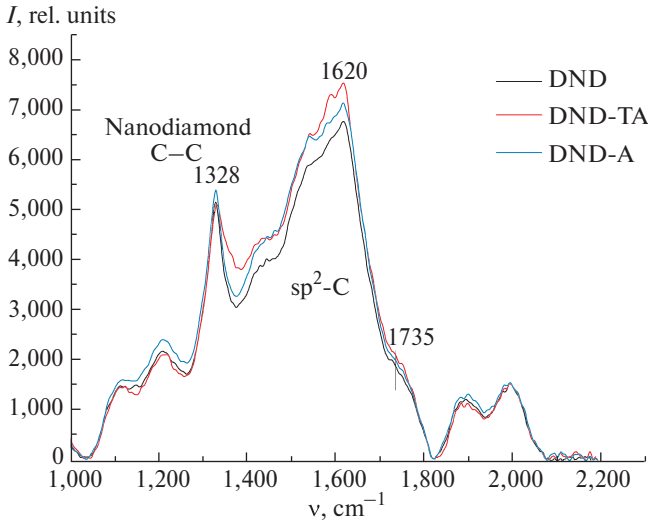


**Fig. 4.** Raman spectra of DND powders.

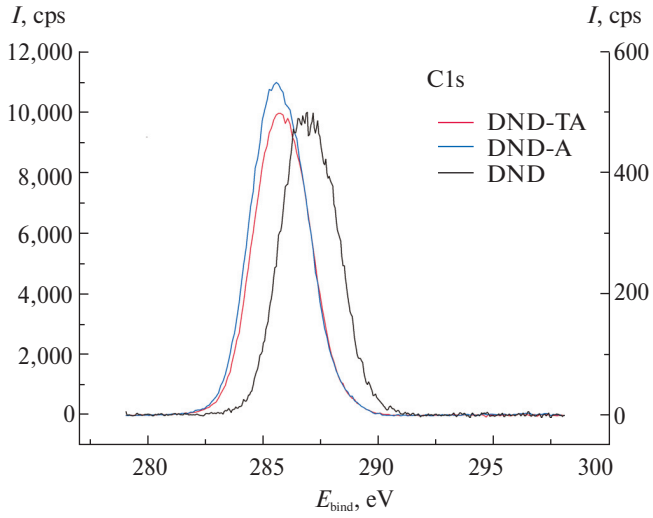


**Fig. 5.** X-ray photoelectron spectra of C1s of DND powders.

all the obtained results on the study of the surface composition, apparently from the bulk graphite-like phase.

From Fig. 7 shows that the O1s spectra for all the studied samples are quite close. When deconvolving the peaks of the O1s spectra (shown on the example of DND-A, Fig. P3 of the Appendix), at a binding energy of 533.1 ± 0.1 eV, the main peak corresponding to bonding between carbon and oxygen atoms in C–O–C and C–O–H groups is observed, as well as a peak of low intensity with a maximum of 530.8 ± 0.1 eV corresponding to the C=O bonding energy in the carbonyl or carboxyl group [35–37, 40].

It is known that surface charging of nanodiamond particles in liquid dispersion medium in the presence of ionogenic carboxyl and hydroxyl functional groups on their surface is described by the following surface reactions [23, 41]:

$$-COH_2^+ \rightleftarrows -COH + H_s^+,$$

$$-COOH \rightleftarrows -COO^- + H_s^+,$$

$$-COH \rightleftarrows -CO^- + H_s^+.$$

Analysis of all obtained results showed that there is an obvious increasing contribution of carboxyl groups to the formation of surface charge of samples with additional acid or thermoammonia treatment in comparison with the initial sample of detonation nanodiamond.

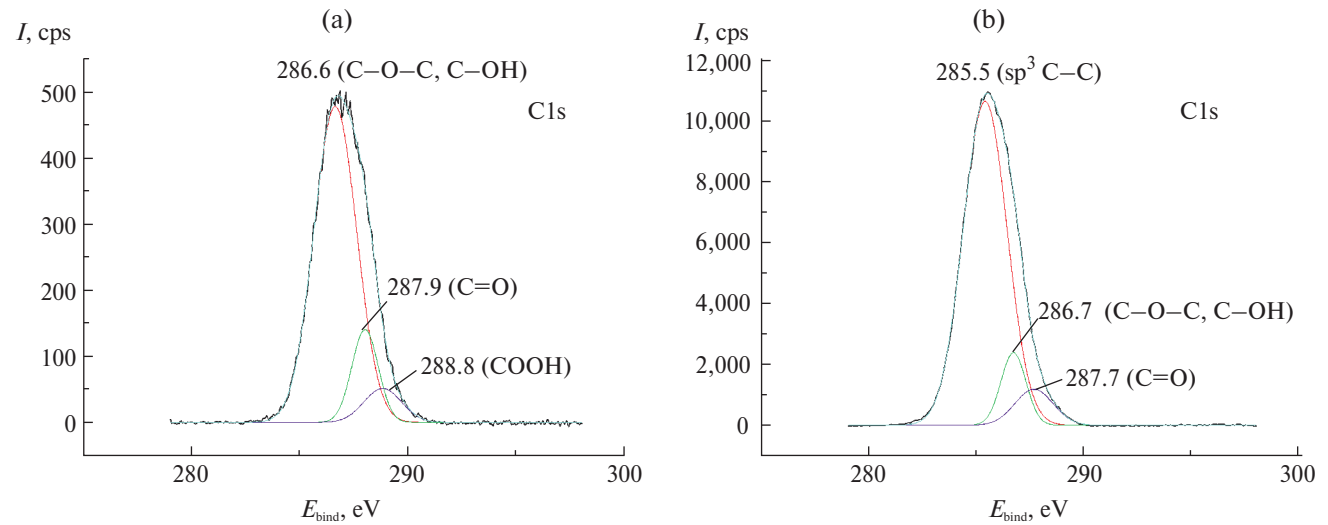


**Fig. 6.** X-ray photoelectron spectra of C1s of DND (a) and DND-A (b) powders.

*Stability and electrokinetic properties of aqueous DND sols in NaCl solutions.*

The study of electrokinetic properties and aggregative stability of aqueous sols of the provided DND powders was initiated in $10^{-3}$ M sodium chloride solution at different pH values. The results of the electrokinetic properties are summarized in Fig. 8 and Table 2. It can be seen that acid treatment of the initial DND powder leads to a shift of the IEP position from pH 7.0 to pH 6.3, and thermoammonia treatment – to pH 6.0, which is in good agreement with the results of the study of the surface composition of these samples: both with an increase in the number of surface carboxyl groups and a decrease in the content of impurities as a result of additional treatment. It can also be seen that the slope of the linear part of the dependences $U_e$ ($\zeta^S$) – log$C$ for DND and DND-TA samples coincides and is equal to about 16 mV/pH unit, and for DND-A is 34 mV/pH unit. It should be noted that at the same offset from IEP ($\Delta pH = pH - pH_{IEP}$) (Fig. P4 of the Appendix) in the region of positive values the values of electrokinetic potentials coincide within the error limits for all investigated DND samples, which is apparently due to the contribution of only hydroxyl functional groups to charge formation (Eq. 3). In the region of negative values, small differences are observed: so the minimum absolute values of zeta-potential correspond to the initial sample, while the maximum values correspond to DND-A. This is probably due to the different degree of influence of surface impurities on the electrokinetic properties of DND particles at pH change, which is mainly manifested in the alkaline pH region, and the different contribution of carboxyl groups to the formation of negative charge.

The results of studying the coagulation kinetics and determining the average particle size of DND sols on the background of $10^{-3}$ M NaCl solution as a function of pH are shown in Fig. 9, P5–P7 of the Appendix and Fig. 10, respectively. It can be seen that rapid coagulation of sols occurs in the region of the isoelectric point, as the distance from it towards higher and lower pH, a transition to the zones of slow coagulation accompanied by a decrease in optical density and average particle size is observed, and then to the regions of aggregative stability. It should be noted that in the region of slow coagulation at some pH a bimodal particle size distribution was observed (the value of average peak sizes in Fig. 10 are connected by a dashed line). As can be seen from Figs. 9 and 10, for aqueous DND-TA and DND-A sols, the zones of aggregative stability practically coincide (hydrosols are stable at pH $\leqslant$ 4.9 and at pH $\geqslant$ 8.4 – regions of positive and negative values of electrokinetic potential, respectively), which is apparently due to the close position of isoelectric points. The shift of the IEP to pH 7.0 for the baseline purification DND causes an extension of the stability zone in the region of positive zeta potential values up to pH 5.8. It should be noted that for the initial DND, in contrast to the samples subjected to additional treatment, no stability in the region of negative values of ζ-potential is observed. Apparently, at high pH values, partial dissolution of surface impurities, which are removed in the case of DND-A and DND-TA during additional treatment, may occur, accompanied by the appearance of multi-charged cations in dispersion medium, which cause coagulation of DND particles. It can also be seen that in the region of negative values of zeta potential in the stability zone for DND-TA and DND-A, in some cases, optical density values are observed even lower

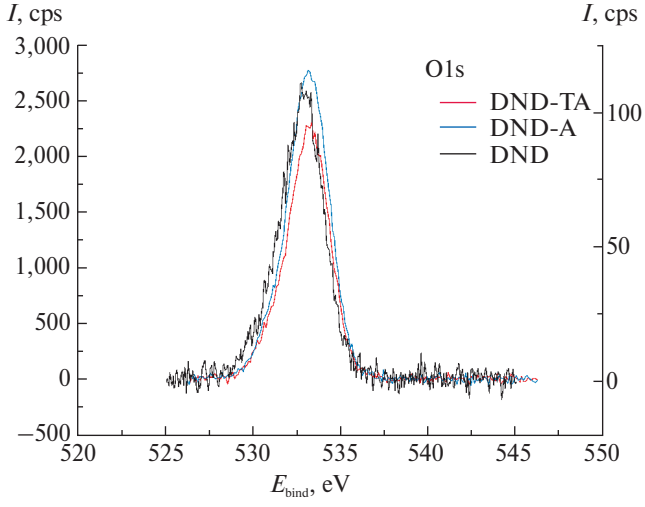


**Fig. 7.** X-ray photoelectron spectra of O1s of DND powders.

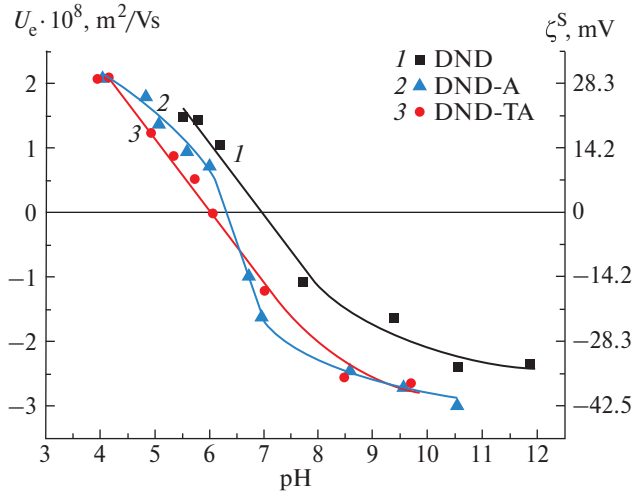


**Fig. 8.** Dependence of electrophoretic mobility (Ue) and electrokinetic potential (ζS) of hydrosol particles of different DND samples on the pH of $10^{-3}$ M sodium chloride solution.

**Table 2.** IEP pH values of DND samples and thresholds of fast and slow coagulation of their hydrosols in NaCl solutions at natural pH value

| Sample | $pH_{IEP}$ ($10^{-3}$ M NaCl) | Threshold of slow coagulation $C_{SC}$, M | Fast coagulation threshold $C_{FC}$, M |
|---|---|---|---|
| DND | 7.0 | $2.5\times10^{-3}$ | $7.5\times10^{-3}$ |
| DND-A | 6.3 | $2.8\times10^{-4}$ | $1.5\times10^{-3}$ |
| DND-TA | 6.0 | – | $\leqslant 10^{-4}$ M |

than for the initial aqueous sol. This, apparently, can be related to the partial disintegration of primary aggregates and the increase in the fraction of smaller particles with increasing absolute values of surface charge and electrokinetic potential.

Due to the fact that most often manufacturers of DND are primarily interested in their stability in aqueous medium at natural pH, coagulation thresholds in sodium chloride solutions were determined for the sols of the studied DND. For this purpose, the coagulation kinetics of DND sols was studied (the results are shown in Figs. 11–13) and the average particle sizes of dispersions were determined (Fig. 14) at different concentrations of NaCl solutions and natural pH 5.8 ± 0.2. On the basis of the obtained kinetic data, concentration dependences of the optical density of sols at 0.5 and 15 minutes of observation were plotted, from which the values of the slow $C_{SC}$ and fast $C_{FC}$ thresholds were found graphically (according to the method described in [29]). An example of the determination of coagulation thresholds is shown in Fig. P8 of the Appendix. The values of threshold electrolyte concentrations thus found are summarized in Table 2. It can be seen that the values of the coagulation thresholds of the studied samples agree well with the results of particle size determination (Fig. 14) and are in good agreement with the provisions of their IEP. Thus, the highest values of zeta potential (Fig. 15) and, accordingly, the thresholds of both slow and fast coagulation are observed for the basic purification DND (Table 2), whereas for the dispersion of DND-TA particles, which are practically in isoelectric state at natural pH, the threshold of slow coagulation could not be determined, and fast coagulation occurs already at a concentration of $10^{-4}$ M. As can be seen, detonation diamond sols are characterized by a rather narrow zone of slow coagulation, possibly due to the relatively high Hamaker constant of DND particles; however, it is noteworthy that additional acid treatment leads to the expansion of the slow coagulation zone of the DND-A sample compared to the initial DND.

Thus, we would like to note that the approach often used to assess the prospects of using DND powders by their stability and zeta potential value in water with

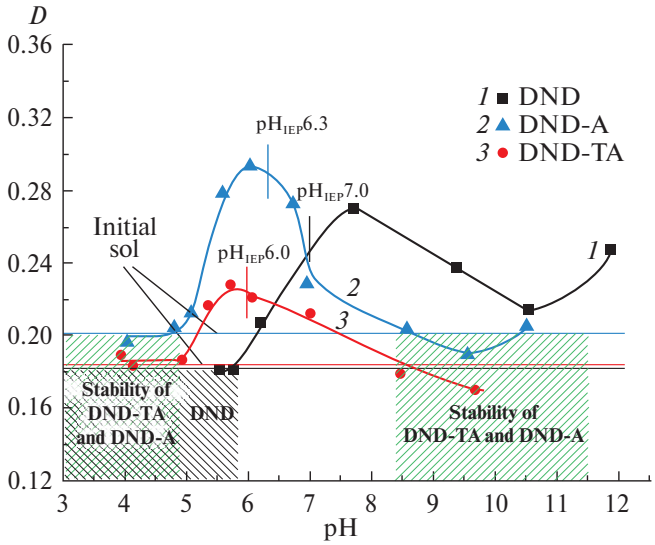


**Fig. 9.** Dependence of the optical density of aqueous detonation diamond sols on the pH of $10^{-3}$ M sodium chloride solution for 15 minutes of observation.

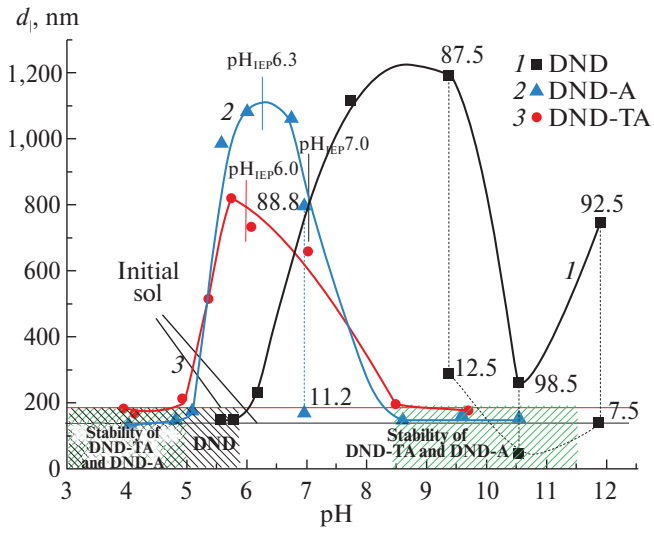


**Fig. 10.** Dependence of the mean DND particle size, determined from the scattered light intensity size distributions, on the pH of $10^{-3}$ M sodium chloride solution for 20 min of observation.

differences in the position of their IEP is incorrect, since, despite the lowest coagulation thresholds, the most promising for further use (e.g., obtaining carboxylated or hydrogenated DND on its basis) seems to be the DND-TA sample.

## CONCLUSION

Analysis of the results of the study of the phase composition and surface composition of detonation diamond particles with different prehistory of production showed that additional acid and especially thermoammonia treatment of initial DND leads to a more complete purification of the surface of DND particles from the non-diamond phase. This leads to an increase in the number of surface protonated carboxyl groups due to both the removal of some impurities remaining in the graphite-like phase after primary treatment and the oxidation of C=C bonds of the $sp^2$-hybridized shell around the diamond core.

It was found that the main contribution to the formation of surface charge for all samples is made by surface dissociation-association reactions of hydroxyl groups, while the increase in the number of carboxyl groups for DND powders with additional treatment and different efficiency of acid and thermoammonia treatment to dissolve different types of surface

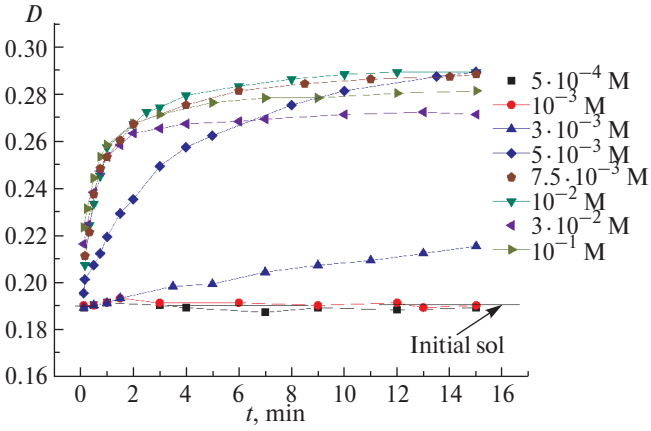


**Fig. 11.** Dependence of the optical density of DND hydrosol on the observation time at different concentrations of sodium chloride solutions and natural pH value.

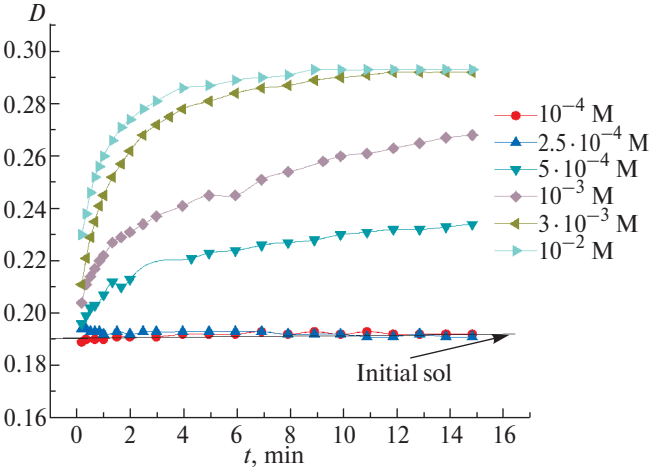


**Fig. 12.** Dependence of optical density of DND-A hydrosol on observation time at different concentrations of sodium chloride solutions and natural pH value.

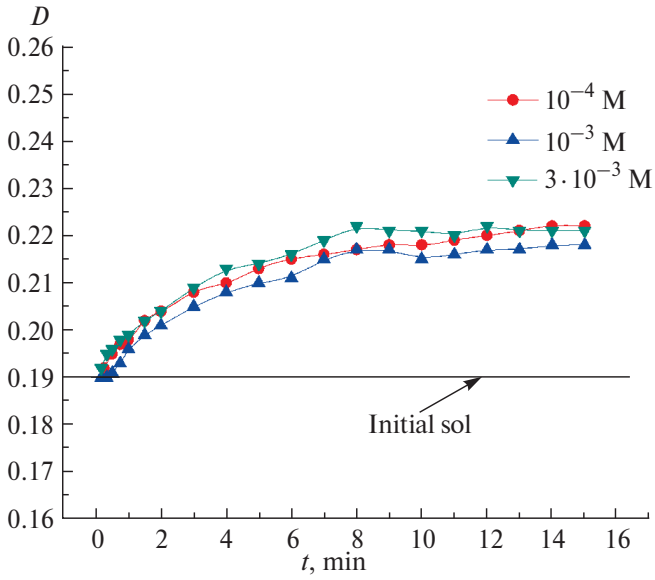


**Fig. 13.** Dependence of optical density of DND-TA hydrosol on observation time at different concentrations of sodium chloride solutions and natural pH value.

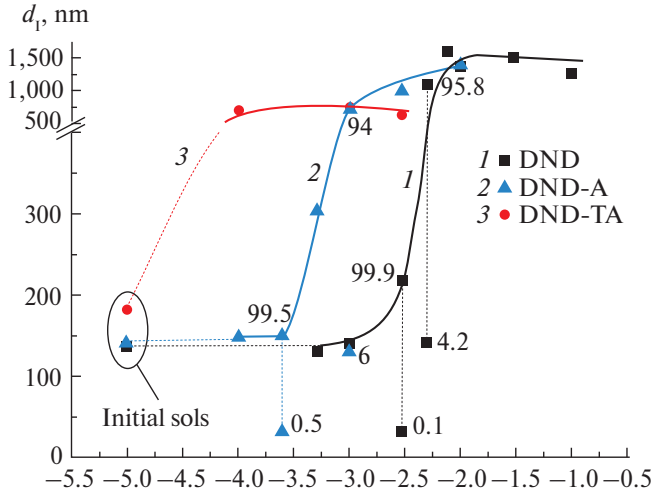


**Fig. 14.** Dependence of the average particle size $d_1$ on the concentration of NaCl solutions at natural pH value. Numerical values at dots are the fraction (%) of light intensity scattered by particles of a given size (given for the case of bimodal distribution).

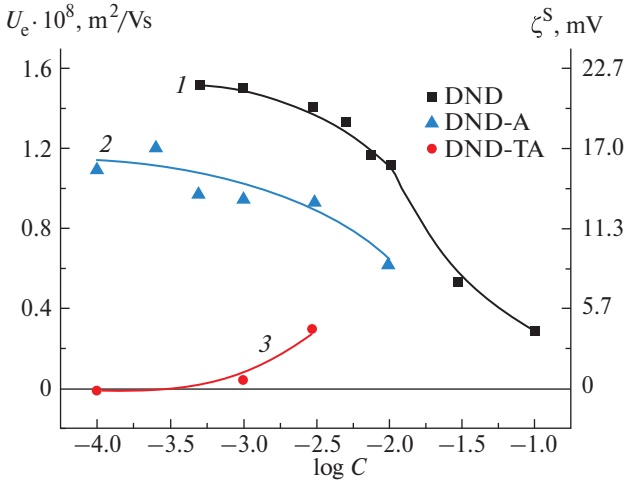


**Fig. 15.** Dependence of electrophoretic mobility ($U_e$) and electrokinetic potential ($\zeta^S$) of hydrosol particles of different DND samples on the concentration of sodium chloride solutions at natural pH value.

impurities leads to differences in the electrokinetic properties and aggregative stability of the studied samples especially in the region of negative values of zeta potential.

It was found that acid treatment of basic purification of DND powder leads to a shift in the position of the isoelectric point from pH 7.0 to pH 6.3, and thermoammonia treatment – to pH 6.0 on the background of $10^{-3}$ sodium chloride solution. The zones of aggregative stability of DND sols were determined: hydrosols of detonation nanodiamond with additional treatment are stable in the region of positive values of electrokinetic potential at pH $\leqslant$ 4.9 and at pH $\geqslant$ 8.4 – in the region of negative ones according to the change of their electrokinetic properties. Aqueous sol of positively charged DND is stable at pH $\leqslant$ 5.8, in the whole investigated region of negative values of ζ-potential the sol coagulates, probably, due to dissolution of part of surface impurities at high pH values and their transfer in ionic form into solution.

The thresholds of slow and fast coagulation in NaCl solutions at natural pH were determined and compared for the studied DND hydrosols. It is shown that the values of coagulation thresholds of the studied samples are in full compliance with the provisions of their IEP.

## FUNDING

The work was financially supported by the RSF grant No. 23-23-00333.

## ETHICS DECLARATION

There are no human or animal studies in this paper.

## CONFLICT OF INTERESTS

The authors declare that they have no conflict of interests.

## ACKNOWLEDGEMENTS

The authors would like to thank D.A. Alexandrov for specific surface measurements. The research was carried out using the equipment of the Interdisciplinary Resource Centre for Nanotechnology, the Centre for Optical and Laser Materials Research, the Centre for Physical Methods of Surface Investigation, the Centre for X-ray Diffraction Studies, and the Centre for Innovative Technologies of Composite Materials at the Research Park of St. Petersburg State University.

## REFERENCES

1. *Dolmatov V.Yu.* Ultrafine detonation synthesis diamonds: properties and applications // Uspekhi himii. 2001. Vol. 70. No. 7. Pp. 686–708. https://doi.org/10.1070/RC2001v070n07ABEH000665
2. *Dolmatov V.Yu.* Detonation nanodiamonds in oils and lubricants // Sverkhtverdye materialy. 2010. Vol. 32. No. 1. Pp. 19–28.
3. *Volkov D.S., Krivoshein P.K., Mikheev I.V., Proskurnin M.A.* Pristine detonation nanodiamonds as regenerable adsorbents for metal cations // Diamond and Related Materials. 2020. Vol. 110. P. 108121. https://doi.org/10.1016/j.diamond.2020.108121
4. *Peristyy A., Paull B., Nesterenko P.N.* Ion-exchange properties of microdispersed sintered detonation nanodiamond // Adsorption. 2016. Vol. 22. Pp. 371–383. https://doi.org/10.1007/s10450-016-9786-9
5. *Aleksenskii A.A., Chizhikova A.S., Kuular V.I. et al.* Basic properties of hydrogenated detonation nanodiamonds // Diamond and Related Materials. 2024. Vol. 142. P. 110733. https://doi.org/10.1016/j.diamond.2023.110733
6. *Turcheniuk K., Mochalin V.N.* Biomedical applications of nanodiamond // Nanotechnology. 2017. Vol. 28. Pp. 252001–252027. https://doi.org/10.1088/1361-6528/aa6ae4
7. *Schrand A.M., Ciftan Hens S.A., Shenderova O.A.* Nanodiamond particles: Properties and perspectives for bioapplications // Critical Reviews in Solid State and Materials Sciences. 2009. Vol. 34. Nos. 1–2. Pp. 18–74. https://doi.org/10.1080/10408430902831987
8. *Rosenholm J.M., Vlasov I.I., Burikov S.A. et al.* Nanodiamond-based composite structures for biomedical imaging and drug delivery // Journal of Nanoscience and Nanotechnology. 2015. Vol. 15. No. 2. Pp. 959–971. https://doi.org/10.1166/jnn.2015.9742
9. *Xu J., Chow E.* Biomedical applications of nanodiamonds: From drug-delivery to diagnostics // SLAS Technology. 2023. Vol. 28. No. 4. Pp. 214–222. https://doi.org/10.1016/j.slast.2023.03.007

10. *Chiganova G.A., Gosudareva E.Yu.* Structure formation in aqueous dispersions of detonation nanodiamonds // Rossiiskie nanotekhnologii. 2016. Vol. 11. Nos. 7–8. Pp. 25–29.
11. *Solovieva K.N., Belyaev V.N., Petrov E.A.* Investigation of the properties of detonation nanodiamonds depending on the technology of deep purification // Yuzhno-Sibirskii nauchnyi vestnik. 2020. Vol. 21. No. 3. Pp. 62–67. https://doi.org/10.25699/SSSB.2020.21.3.010
12. *Solovieva K.N., Belyaev V.N., Petrov E.A.* Fundamentals of the technology of finishing purification of detonation nanodiamonds // Vestnik tekhnologicheskogo universiteta. 2019. Vol. 22. No. 12. Pp. 85–87.
13. *Shenderova O., Petrov I., Walsh J. et al.* Modification of detonation nanodiamonds by heat treatment in air // Diamond & Related Materials. 2006. Vol. 15. Pp. 1799–1803. https://doi.org/10.1016/j.diamond.2006.08.032
14. *Sharin P.P., Sivtseva A.V., Popov V.I.* Thermal oxidation in air of diamond nanopowders obtained by mechanical grinding and detonation synthesis // Izvestija vuzov. Poroshkovaya metallurgiya i funkcional'nye pokrytiya. 2022. No. 4. Pp. 67–83. https://doi.org/10.17073/1997-308X-2022-4-67-83
15. *Osswald S., Yushin G., Mochalin V. et al.* Control of $sp^2/sp^3$ carbon ratio and surface chemistry of nanodiamond powders by selective oxidation in air // Journal of the American Chemical Society. 2006. Vol. 128. Pp. 11635–11642.
16. *Kulakova I.I.* Modification of detonation nanodiamond: effect on its physico-chemical properties // Rossiyskiy khimicheskiy zhurnal. 2004. Vol. 48. No. 5. Pp. 97–106.
17. *Arnault J.C., Girard H.A.* Hydrogenated nanodiamonds: Synthesis and surface properties //Current Opinion in Solid State and Materials Science. 2017. Vol. 21. Pp. 10–16. https://doi.org/10.1016/j.cossms.2016.06.007
18. *Williams O.A., Hees J., Dieker C. et al.* Size-dependent reactivity of diamond nanoparticles // ACS Nano. 2010. Vol. 4. No. 8. Pp. 4824–4830. https://doi.org/10.1021/nn100748k
19. *Gines L., Sow M., Mandal S. et al.* Positive zeta potential of nanodiamonds // Nanoscale. 2017. Vol. 9. Pp. 12549–12555. https://doi.org/10.1039/C7NR03200E
20. *Terada D., Osawa E., So F. et al.* A simple and soft chemical deaggregation method producing single-digit detonation nanodiamonds // Nanoscale Adv. 2022. Vol. 4. Pp. 2268–2277. https://doi.org/10.1039/D1NA00556A
21. *Batsanov S.S., Dan'kin D.A., Gavrilkin S.M. et al.* Structural changes in colloid solutions of nanodiamond // New J. Chem. 2020. Vol. 44. Pp. 1640–1647. https://doi.org/10.1039/C9NJ05191K
22. *Petrova N., Zhukov A., Gareeva F. et al.* Interpretation of electrokinetic measurements of nanodiamond particles // Diamond and Related Materials. 2012. Vol. 30. Pp. 62–69. https://doi.org/10.1016/j.diamond.2012.10.004
23. *Gareeva F., Petrova N., Shenderova O., Zhukov A.* Electrokinetic properties of detonation nanodiamond aggregates inaqueous KCl solutions // Colloids and Surfaces A: Physicochem. Eng. Aspects. 2014. Vol. 440. Pp. 202–207. https://doi.org/10.1016/j.colsurfa.2012.08.055
24. *Zhukov A.N., Shvidchenko A.V., Yudina E.B.* Electrical surface properties of detonation nanodiamond hydrosols depending on the size of dispersed particles // Colloid Journal. 2020. Vol. 82. No. 4. Pp. 416–422. https://doi.org/10.31857/S0023291220040175
25. *Sychev D.Yu., Zhukov A.N., Golikova E.V., Sukhodolov N.G.* The effect of simple electrolytes on the coagulation of monodisperse negatively charged detonation nanodiamond hydrosols // Colloid Journal. 2017. Vol. 79. No. 6. Pp. 785–791. https://doi.org/10.7868/S0023291217060118
26. *Mchedlov-Petrossyan N.O., Kamneva N.N., Marynin A.I. et al.* Colloidal properties and behaviors of 3 nm primary particles of detonation nanodiamonds in aqueous media // Phys. Chem. Chem. Phys. 2015. Vol. 17. Pp. 16186–16203. https://doi.org/10.1039/C5CP01405K
27. *Mchedlov-Petrossyan N.O., Kamneva N.N., Kryshtal A.P. et al.* The properties of 3 nm-sized detonation diamond from the point of view of colloid science // Ukr. J. Phys. 2015. Vol. 60. Pp. 932–937. https://doi.org/10.15407/ujpe60.09.0932
28. *Mchedlov-Petrossyan N.O., Kriklya N.N., Kryshtal A.P. et al.* The interaction of the colloidal species in hydrosols of nanodiamond with inorganic and organic electrolytes // Journal of Molecular Liquids. 2019. Vol. 283. Pp. 849–859. https://doi.org/10.1016/j.molliq.2019.03.095
29. *Volkova A.V., Beloborodov A.A., Vodolazhskii V.A. et al.* Effect of pH and concentration of an indifferent electrolyte on the aggregative stability of an aqueous detonation diamond sol // Colloid Journal. 2024. Vol. 86. No. 2. Pp. 169–192. https://doi.org/10.31857/S0023291224020031
30. *Petit T., Puskar L.* FTIR spectroscopy of nanodiamonds: Methods and interpretation // Diamond & Related Materials. 2018. Vol. 89. Pp. 52–66. https://doi.org/10.1016/j.diamond.2018.08.005
31. *Shenderova O., Panich A.M., Moseenkov S. et al.* Hydroxylated detonation nanodiamond: FTIR, XPS, and NMR studies // Phys. Chem. C. 2011. Vol. 115. No. 39. Pp. 19005–19011. https://doi.org/10.1021/jp205389m
32. *Stehlik S., Mermoux M., Schummer B. et al.* Size effects on surface chemistry and Raman spectra of sub-5 nm oxidized high-pressure high-temperature and detonation nanodiamonds // J. Phys. Chem. C. 2021. Vol. 125. Pp. 5647–5669. https://doi.org/10.1021/acs.jpcc.0c09190

33. *Aleksenskiy A.E., Baidakova M.V., Vul` A.Ya., Siklitskiy V.* The structure of the diamond nanocluster // Fizika tverdogo tela. 1999. Vol. 41. No. 4. Pp. 740—743.
34. *Sharin P.P., Sivtseva A.V., Yakovleva S.P. et al.* Comparison of morphological and structural characteristics of nanopowder particles obtained by grinding natural diamond and detonation synthesis method // Izvestiya vuzov. Poroshkovaya metallurgiya i funktsional'nye pokrytiya. 2019. Vol. 4. Pp. 55–67. https://doi.org/10.17073/1997-308X-2019-4-55-67
35. *Frese N., Mitchell S.T., Bowers A. et al.* Diamond-like carbon nanofoam from low-temperature hydrothermal carbonization of a sucrose/naphthalene precursor solution // C Journal of Carbon Research. 2017. Vol. 3. No. 3. P. 23. https://doi.org/10.3390/c3030023
36. *Lim D.G., Kim K.H., Kang E. et al.* Comprehensive evaluation of carboxylated nanodiamond as a topical drug delivery system // International Journal of Nanomedicine. 2016. Vol. 11. Pp. 2381–2395. https://doi.org/10.2147/IJN.S104859
37. *Thomas A., Parvathy M.S., Jinesh K.B.* Synthesis of nanodiamonds using liquid-phase laser ablation of graphene and its application in resistive random access memory // Carbon Trends. 2021. Vol. 3. P. 100023. https://doi.org/10.1016/j.cartre.2020.100023
38. *Petit T., Arnault J.C., Girard H.A. et al.* Early stages of surface graphitization on nanodiamond probed by x-ray photoelectron spectroscopy // Physical Review B – Condensed Matter and Materials Physics. 2011. Vol. 84. No. 23. P. 233407. https://doi.org/10.1103/PhysRevB.84.233407
39. *Lan G., Qiu Y., Fan J. et al.* Defective graphene@ diamond hybrid nanocarbon material as an effective and stable metal-free catalyst for acetylene hydrochlorination // Chemical Communications. 2019. Vol. 55. Pp. 1430–1433. https://doi.org/10.1039/C8CC09361J
40. *Testolin A., Cattaneo S., Wang W. et al.* Cyclic voltammetry characterization of Au, Pd, and AuPd nanoparticles supported on different carbon nanofibers // Surfaces. 2019. Vol. 2. No. 1. Pp. 205–215. https://doi.org/10.3390/surfaces2010016
41. *Zhukov A.N., Gareeva F.R., Aleksenskiy A.E.* A comprehensive study of the electrical surface properties of detonation nanodiamond agglomerates in aqueous solutions of KSd // Colloid Journal. 2012. Vol. 74. No. 4. Pp. 483–491.